Contact law in granular assemblies: from statics to dynamics

Lingran Zhang, Stéphane Lambert, François Nicot, Franck Bourrier

Contact law in granular assemblies: from statics to dynamics

L. Zhang, S. Lambert, F. Nicot
Irstea, UR ETGR, 2 rue de la Papeterie-BP76, F-38402 Saint Martin d'Hères, France

F. Bourrier
Irstea, UR EMGR, 2 rue de la Papeterie-BP76, F-38402 Saint Martin d'Hères, France

ABSTRACT: In this paper, we investigate the efficiency of a numerical model including rolling resistance for considering dynamical impact loading problems. For this purpose, a discrete element method is considered in a three dimensional context, and the granular assembly is composed by non-cohesive poly-disperse spherical particles. First, triaxial test simulations were conducted for model calibration purpose. Second, the impact modeling of a projectile falling onto a granular layer was conducted using the calibrated model. Particular attention is placed on the influence of the rolling resistance on the system response in both static and dynamic cases. The results indicate that the contact law is acceptable in modeling both static and dynamic cases, besides it has benefits of introducing rolling resistance due to the consideration of the shape of the particles.

1 INTRODUCTION

Rockfall constitutes a major threat in mountainous regions since it causes serious damage to residential areas and infrastructures. When a boulder detaches from the cliff, it encounters different soil bodies on its trajectory down the slope. These can either be natural or man-made, covering the slope or constituting protection structures. Thus, both the whole trajectory of the boulder and the response of the structures are governed by the interaction between the boulder and soil bodies.

Over the past decades, discrete element methods – DEM- have been used to study both quasi-static and dynamic behaviors of granular material such as soils (Cundall & Strack 1979, Ciamarra et al. 2004, Calvetti et al. 2005, Belheine et al. 2009, Plassiard et al. 2009a, b, Kondic et al. 2012). In DEM, the macroscopic response of a granular assembly is governed by the contact law between adjoining particles. This law relates the contact forces to the relative displacements of the particles. In each calculation loop, the positions of particles are first detected and contact forces are computed according to the contact law, then Newton's second law is solved to update the positions of the particles. In DEM, the most simple and frequently used contact law considers a linear relation between the inter-particular penetration and the force in the normal direction and obeys the Mohr-coulomb's criteria in the shear direction.

Most often, the shapes of the particles are not accounted for in DEM: particles are modeled as spherical particles or disks allowing saving computational time. Since the shapes of particles may strongly influence the response of the granular assembly, Iwashita & Oda (1998) considered a rolling resistance law between contacted particles with the aim of modeling the roughness effect. They succeeded in reproducing large voids inside a shear band as well as the high gradient of particle rotation along the shear band boundaries. This approach has also been considered by authors such as Plassiard et al. (2009a), Belheine et al. (2009), who implemented rolling resistance into the classical contact law and used it to model triaxial tests. Besides, impacts of projectiles on granular layers have been investigated by many authors using DEM, different granular materials and impact conditions are considered (Tsimring & Volfson 2005, Wada et al. 2005, Bourrier et al. 2008, Ciamarra et al. 2008, Plassiard & Donzé 2009).

In this paper, we investigate the efficiency of a DEM model considering rolling resistance and calibrated under a static loading path in dealing with localized dynamical loadings. The free open source DEM code YADE is used (Šmilauer et al. 2010). The quasi-static behavior is studied in terms of drained triaxial tests, while dynamic behavior is studied in terms of impact on a granular layer. The

granular assembly is composed of non-cohesive poly-disperse spherical particles. Although soils encountered in rockfall issues are coarse, choice is made to consider a finer experimental analogous material on which triaxial test results were available. It is thus assumed that the soil response along a drained traxial loading path is not modified by this change of scale. Particular attention is placed on the influence of the rolling resistance on the system response in both static and dynamic cases.

2 CONTACT LAW

The normal contact force F_n and shear contact force F_s of the classical contact law are described as equations (1) - (5).

$$F_n = k_n * u_n \quad (1)$$

$$\mathrm{d}F_s = k_s * \mathrm{d}u_s \quad (2)$$

$$F_s \leq tan\varphi * F_n \quad (3)$$

$$k_n = 2 * \frac{K_A^n * r_A * K_B^n * r_B}{K_A^n * r_A + K_B^n * r_B} \quad (4)$$

$$k_s = 2 * \frac{K_A^s * r_A * K_B^s * r_B}{K_A^s * r_A + K_B^s * r_B} \quad (5)$$

where k_n is the normal stiffness, k_s is the shear stiffness, r_A and r_B are the radii of particles A and B respectively, u_n is the overlap in the normal direction between the two particles, $\mathrm{d}u_s$ is the shear incremental displacement, φ is the friction angle between particles. K_A^n and K_B^n are the normal local modulus of particle A and B, K_A^s and K_B^s are the tangential local modulus of particle A and B. In our simulations, $K_A^n = K_B^n$, $K_A^s = K_B^s$.

The implemented rolling resistance follows the theory proposed by Iwashita and Oda (1998). The bending resistance, M_r, is computed incrementally as follows:

$$\mathrm{d}M_r = k_r * \mathrm{d}\theta_r \quad (6)$$

where $\mathrm{d}M_r$ is the incremental rolling moment, k_r is the rolling stiffness, β_r is the rolling stiffness coefficient, $\mathrm{d}\theta_r$ is the relative rotation angle between the two particles.

$$k_r = \beta_r * k_s * r_A * r_B \quad (7)$$

and

$$\mathrm{d}\theta_r = (\omega_A * r_A - \omega_B * r_B) * dt * \vec{s} \quad (8)$$

ω_A and ω_B are the angular velocities of A and B, dt is the time step, $\vec{s}$ is a unit vector parallel to the shear contact direction. Contrary to the initial model, no threshold is considered for M_r.

3 QUASI-STATICS CALIBRATION

3.1 Description of the tests

The model calibration is based on drained triaxial tests conducted on Ticino sand (Salot et al. 2009). This sand is angular (20% and 55% by mass of the particles are angular and subangular respectively) The friction angle is 41.8°.

The numerical sample was prepared following a two-step procedure: (i) generation of the poly-disperse particle assembly within the specimen boundaries and (ii) increase of the particles radii to reach the targeted isotropic confinement of 99kPa.

Figure 1 shows the grain size distribution of the numerical particles and the numerical specimen after isotropic confinement. The size of the specimen is 2.9m × 5.8m × 2.9m, the number of the particles is 10000. The density of the specimen is 1631 kg/m^3, the porosity is 0.373.

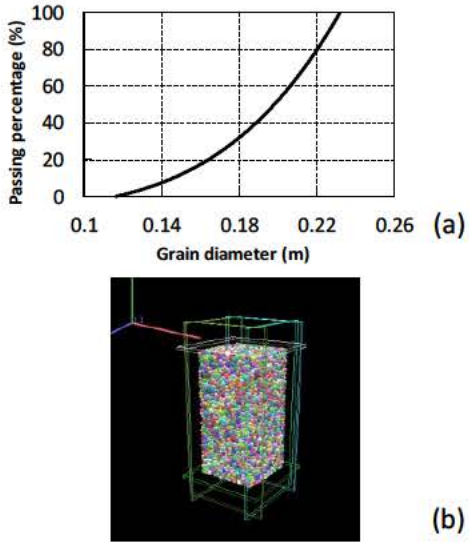

Figure 1. (a) Grain size distribution of the sand particles and (b) numerical specimen after isotropic confinement

3.2 Calibration and Results

The calibration is based on both the deviatoric stress and the volumetric strain evolution in terms of the axial strain. Calibration concerns the normal local modulus K^n, ratio of K^s/K^n, internal friction angle φ, and rolling stiffness coefficient β_r. K^n and K^s/K^n control the sample Young modulus

and Poisson's ratio. φ influences the peak strength as well as dilatancy. β_r has similar effects as φ.
First, K^n and K^s/K^n were calibrated by matching with macroscopic Young modulus and Poisson's ratio. Second, φ was adjusted to reproduce the volumetric strain while keeping other parameters constant. Third, β_r was calibrated to match the stress-strain curve.
The calibrated microscopic parameters are given in table 1.

Table 1. Values of calibrated microscopic parameters for triaxial simulation

Parameters	Values
Normal local modulus K^n(MPa)	100
Ratio K^s/K^n	0.3
Internal friction angle φ (°)	45
Rolling stiffness coefficient β_r	0.2

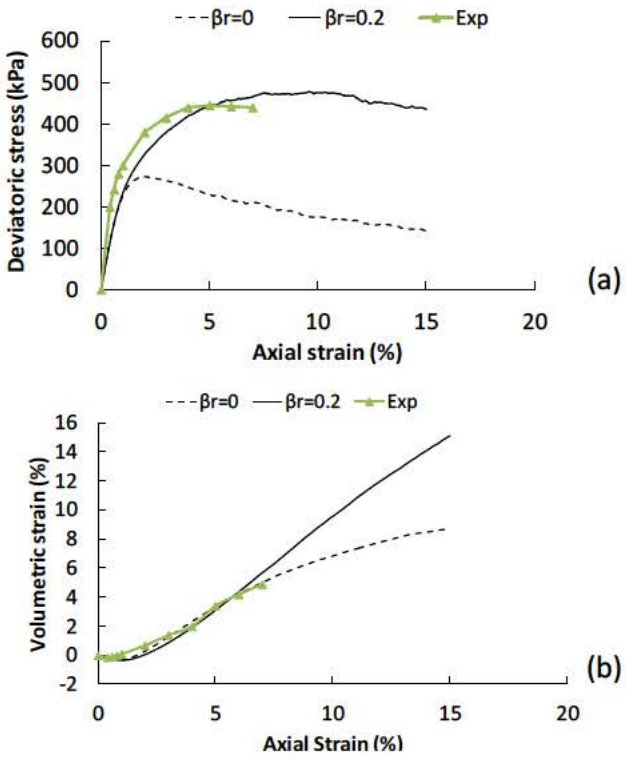

Figure 2. Deviatoric stress (a) and volumetric strain (b) versus axial strain under 99kPa confining pressures for two values of β_r and comparison with experimental values.

Figure 2 shows the curves of deviatoric stress and volumetric strain as functions of axial strain. Curves corresponding to the case without rolling resistance ($\beta_r = 0$) where obtained using the same K^n, K^s/K^n and φ values allowing showing the influence of rolling resistance.
The agreement between simulation results and experiments are good when rolling resistance is considered (figure 2). Without rolling resistance, the deviatoric stress peak is reached at a smaller axial strain around 2%, and the corresponding deviatoric stress is reduced by about 40% compared to the case with rolling moment. Besides, the post-peak softening is more pronounced without rolling resistance. These differences demonstrate the strong influence of the rolling resistance on the triaxial response of the sand.
Figure 3 shows the results of triaxial tests at confining pressures of 99, 200 and 300 kPa. The deviatoric stress peak values as well as the volumetric strain obtained from the simulations are in accordance with experimental values. The agreement is less good concerning the axial strain at peak. And, the higher the confining pressure the higher the difference between experimental and numerical values. Even though, the calibrated parameters are considered satisfying enough to model the soil's response.

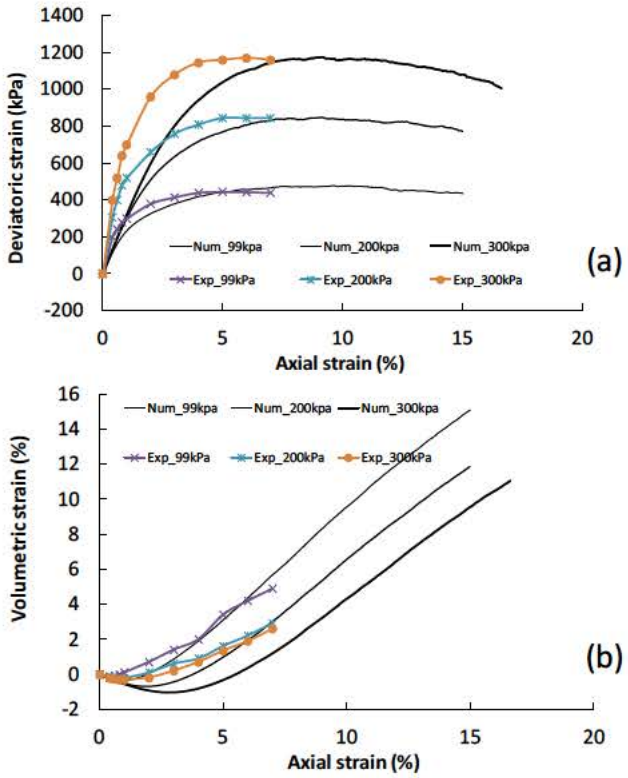

Figure 3. Deviatoric stress (a) and volumetric strain (b) versus axial strain for experiments and simulations under different confining pressures

4 IMPACT SIMULATIONS

4.1 Impact simulation model

The simulation concerns a projectile impacting a granular layer. The same grain size distributions, contact laws and parameters as for the static test were used. The granular layer consisted of 200000 particles and was 20m × 20m × 3.89m in

dimensions (i.e. typically 20 particles along the vertical axis). The granular layer was obtained by gravity deposition. The friction angle between particles was set to zero during deposition in order to obtain a dense layer (the density was 1605 kg/m^3 after deposition). The granular layer was leaned on a rigid and smooth surface, referred as 'bottom' hereafter.

The projectile was modeled as a sphere with a radius Rb either 5 or 7 times the mean radius Rm of granular particles (Rm=0.1m). The projectile was positioned just above the granular layer in the center of the sample (Figure 4). The projectile was given an initial vertical velocity, Vz0, (10, 16.6 or 20m/s). This range is consistent with the velocity range observed for rock boulders along natural slopes. The distance between the impact point and the lateral boundaries of the soil layer was 2.5 times the distance from the impact point to the bottom. This ratio was large enough to limit the effects of the lateral boundaries.

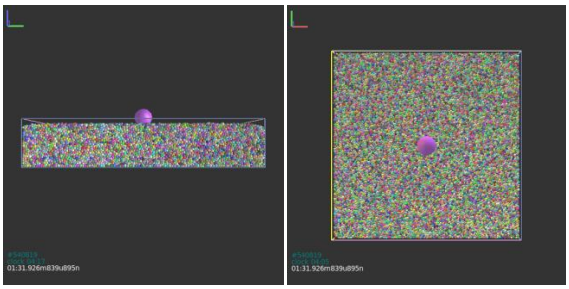

Figure 4. Representations of the projectile and the granular layer

4.2 Impact simulations results

Figure 5 gives simulation results for Rb=5*Rm and V_{z0}=20m/s, with and without rolling resistance. Simulation results are given in terms of vertical component of the forces acting on the projectile, F_{boul}; vertical projectile velocity, Vz; displacement of the projectile from the impact beginning, Z; kinetic energy of the granular layer Ek and energy dissipation of the whole system Ed.

In both cases, F_{boul} rapidly increases to reach a maximum value about 14 ms after the impact begining. On the whole, the impact lasts about 42 ms. F_{boul} is slightly smaller without rolling resistance.

Figures 5 (b) and (c) reveal a significant influence of rolling resistance on the penetration. In particular, a rebound is observed when the rolling resistance is accounted for, while the projectile keeps going downwards before stopping when rolling resistance is not accounted for. The rebound lasts about 180 ms, during which there is no contact between the projectile and the granular layer. The final penetrations of the projectile in the granular layer (i.e. position at rest) in the two cases are 0.33m and 0.77 m respectively. It is worth noting that when accounting for the rolling resistance, the penetration of the projectile during the first impact is only 0.28 m, the projectile impacts again the soil at a position of 0.37 m. The soil keeps going downwards between the first two impacts. On the contrary, in the case without rolling resistance, the soil keeps moving downwards, the projectile remains in rather close and constant contact with the granular layer. The force acting on the projectile is rather small. When rolling resistance is not accounted for, impact on spheres leads to cratering which is in accordance with previously published results (Wada et al. 2006, Ciamara et al. 2004).

From Figures 5 (d) and (g) it can be shown that without rolling resistance both the kinetic energy and energy dissipation are much higher than with rolling resistance. Figure 5 (f) gives, $\widehat{\widehat{E}}$, the relative variation of the sum of the different energy terms (strain, kinetic, potential and dissipation). It shows that divided by the total is rather constant during the simulations.

The force acting on the bottom started increasing about 18 ms after the force on the boulder started increasing. This time lag leads to a 210 m/s compression wave velocity which is consistent with the expected order of magnitude. The maximum value of the dynamic forces acting on the bottom, ΔF_{bot}, is about 3 times the maximum impact force which is consistent with experimental results (Stoffel 1988, Calvetti & di Prisco 2005).

In addition, different projectile's radii and impact velocities are considered (table 2). With both models, the maximum value of F_{boul} is proportional to the projectile velocity (test 1 vs 3). Comparison of the two models indicates that without rolling resistance, F_{boul} is always smaller, ΔF_{bot} is always smaller and the penetration is always higher. In terms of penetration, a small projectile with a high velocity (test 3) will result in a similar penetration as a large projectile of smaller velocity with a smaller kinetic energy (test 2). By comparison with test 2, test 4 reveals that for a same kinetic energy in the case of without rolling resistance, the penetration decreases with the increasing of the projectile's radius which differs from experimental observations.

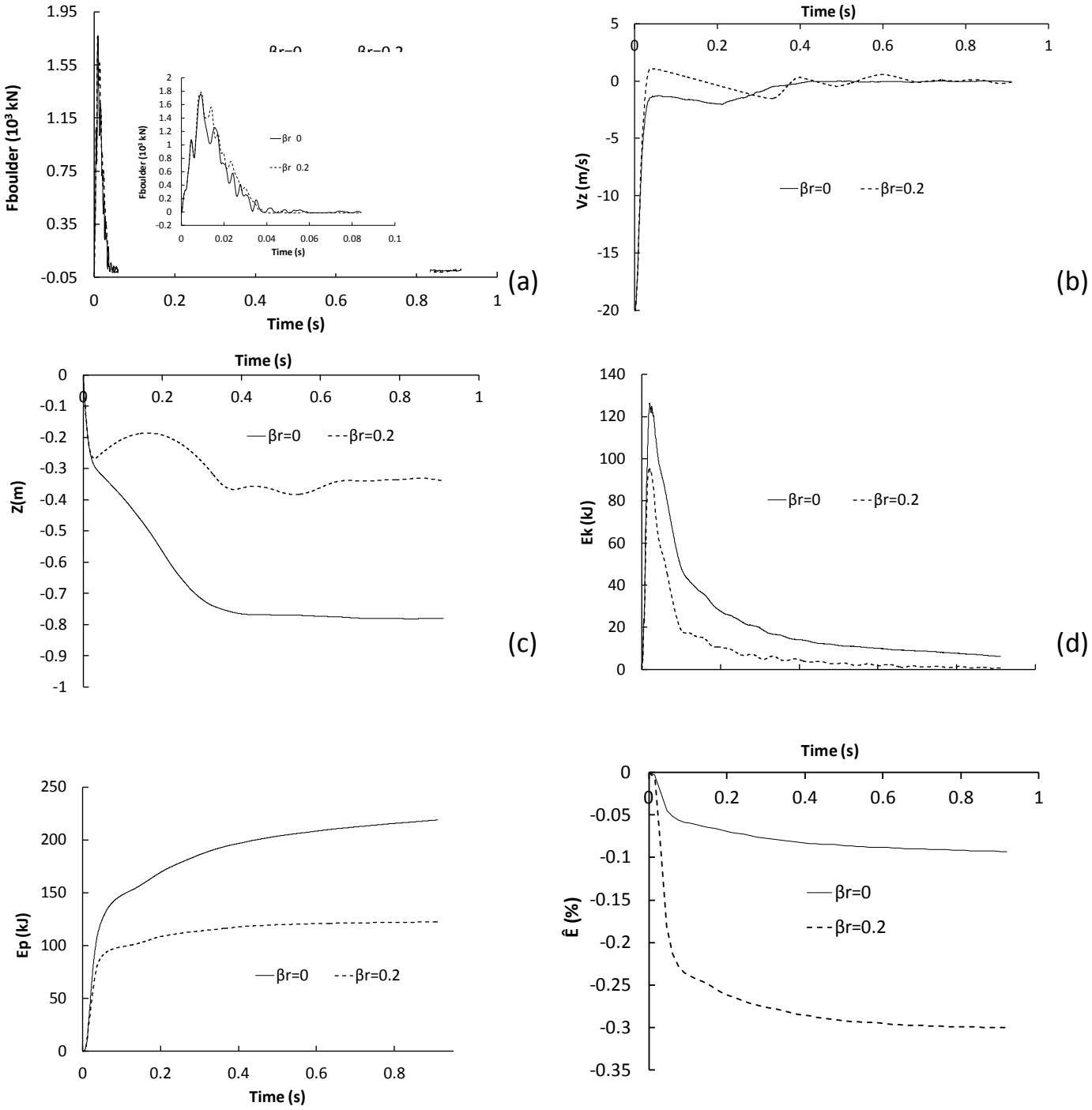

Figure 5. Numerical results in terms of (a) F_{boul}, (b) Vz, (c) Z, (d) Ek, (e) Ed and (f) $\overline{E}$ in case of Rb=0.5m, Vz_0=20 m/s

Table 2. Numerical results for different boulder sizes and different impact velocities

Tests	Rb (m)	V (m/s)	Ek (kJ)	Max.(F_{boul}) (kN)		Max.(ΔFbot) (kN)		Final penetration (m)	
				=0.0	=0.2	=0.0	=0.2	=0.0	=0.2
1	0.5	10	68	629	728	2404	2551	0.47	0.23
2	0.7	10	187	912	1138	3865	4462	0.78	0.34
3	0.5	20	272	1757	1786	5537	5736	0.77	0.33
4	0.5	16.6	187	1403	1446	4451	4671	0.69	0.34

4.2 Discussion

In the absence of specific experiments, comparison with experiments in similar context could be conducted. In particular, Stoffel (1998) conducted impact experiments on a granular layer lying on a concrete slab. The experimental impact duration is similar to that of the simulations. This author also proposed a relation between the force acting on the projectile and the projectile penetration:

$$\frac{}{\mathrm{ax}(F \quad r)} \tag{9}$$

with

$$\exp(\text{——}) \tag{10}$$

where E_k is the initial kinetic energy of the projectile and H is depth of the granular layer.
In the case of test 3 (Fig. 5), this relation gives a penetration value of 0.249 and 0.253 m for the cases with and without rolling resistance respectively. This comparison show that the 0.77 m penetration obtained without rolling resistance is not realistic, contrary to the 0.33m penetration obtained with rolling resistance.
The results globally reveal the influence of the rolling resistance on the granular layer response. Similarly to the angularity effect, rolling resistance influences the relative displacement of adjoining particles. To some extent, it can be considered that it improves the stability of force chains. In the absence of rolling resistance, the granular assembly is less stable. As a consequence, the kinetic energy of the boulder that is transferred to the granular packing rapidly leads to a granular layer kinetic energy increase, with only limited energy stored as strain energy. The higher kinetic energy results in an higher energy dissipation, by friction. By contrast, accounting for rolling resistance leads to a higher ratio of strain energy within the granular assembly, a limited kinetic energy and thus a smaller dissipation.

5 CONCLUSIONS

In this paper, we investigate the efficiency of a classical contact law implemented with rolling resistance calibrated under a static triaxial loading path, and in dealing with dynamical impact loading problems. First, triaxial tests were conducted for model calibration purpose. Second, dynamic loading of projectiles impacting on a granular layer using the same calibrated model was conducted. Results in both static and dynamic cases are tracked and analyzed. Particular attention has been focused on the influence of rolling resistance on the response of the system in both cases. The results indicate:

1. The calibrated contact law is acceptable in modeling both static and dynamic loadings.
2. Rolling resistance is a powerful gradient to improve the peak strength in triaxial tests.
3. Rolling resistance shows a significant influence on the penetration in dynamic impacts.

6 REFERENCES

Bourrier, F., Nicot, F., & Darve, F. 2008. Physical processes within a 2D granular layer during an impact. Granular Matter 10: 415-437.

Belheine, N., Plassiard, J. P., Donzé, F.V. & Darve, F. 2009. Numerical simulation of drained triaxial test using 3D discrete element modeling. Computers and Geotechnics 36: 320-331.

Calvetti, F. Di Prisco, C. & Vecchiotti, M. 2005. Experimental and numerical study of rock-fall impacts on granular soils. Rivista Italiana di Geotecnica 4: 95–109.

Ciamarra, M. P., Lara, A. H., Lee, A. T., Goldman, D. I., Vishik, I. & Swinney, H. L. 2004. Dynamics of drag and force distributions for projectile impact in a granular medium. Phys. Rev. Lett. 92, 194301.

Cundall, P.A.& Strack, O.D.L. 1979. A discrete numerical model for granular assemblier. Geotechnique 29(1): 47-65.

Iwashita, K & Oda, M. 1998. Rolling resistance at contacts in simulation of shear band development by DEM. - Journal of engineering mechanics. J. Eng. Mech. Div., 124 (3), ASCE: 285-292.

Kondic, L., Fang, X., Losert, W., O'Hern, C. S., Behringer, R. P. 2012. Microstructure evolution during impact on granular matter. Physical review. E85, 011305.

Plassiard, J. P, Belheine, N. & Donze, F.V. 2009a. A spherical discrete element model: calibration procedure and incremental response. Granular Matter. 11: 293-306.

Plassiard J. P. & Donze, F.V. 2009b. Rockfall Impact Parameters on Embankments: A Discrete Element method Analysis. Structural Engineering International. 19: 333–341.

Salot, C., Gotteland, P. & Villard, P. 2009. Influence of relative density on granular materials behavior: DEM simulations of triaxial tests. Granular Matter 11:221-236

Šmilauer, V., Catalano, E. Chareyre, B., Dorofeenko, S., Duriez, J., Gladky, A., Kozicki, J., Modenese, C, Scholtès, Sibille, L. , Stránský, J. , and Thoeni, K. Yade Documentation (V. Šmilauer, ed.), The Yade Project, 1st ed., 2010. http://yade-dem.org/doc/.

Stoffel, S. M. 1998. Sollicitation dynamique de la couverture des galeries de protection lors de chutes de blocs. Thèse N◦ 1899, EPFL.

Wada, K., Senshu, H. & Matsui, T. 2006. Numerical simulation of impact cratering on granular material. Icarus 180 (2600): 528-545.